INVESTIGATION OF UNSTEADY FLOWS IN A CENTRIFUGAL FAN USING HIGH-SPEED PIV AND NUMERICAL SIMULATIONS

Andreas LUCIUS[1], Andreas LEHWALD[2], Gunther BRENNER[1], Dominique THÉVENIN[2]

[1] *Clausthal University of Technology, Institute of Applied Mechanics, Adolp-Roemer Str. 2A, 38678 Clausthal-Zellerfeld, Germany*

[2] *University "Otto von Guericke", Lab. of Fluid Dynamics & Technical Flows, Universitätsplatz 2, 39106 Magdeburg, Germany*

SUMMARY

In the present paper the flow field in the rotor of a centrifugal fan is analysed using High-Speed Particle Image Velocimetry and numerical simulations. The measurements show strong thickening of the boundary layer on the suction side, indicating flow separation at design point. With reduced flow rate vortical structures dominate the flow field. The main purpose of the PIV measurements is to provide the unsteady velocity field in the rotor for validation of numerical modelling. The aim of the study is to evaluate the potential of the Scale Adaptive Simulation (SAS) approach for turbulence modelling against a standard RANS (Reynolds Averaged Navier Stokes) and U(nsteady) RANS model respectively. Unsteady flow features are especially investigated using spectral analysis. In addition the computed fluctuating forces on the impeller are analysed. The unsteady forces are of vital importance for the generation of flow-induced vibrations. For the operating points considered the difference of the time-averaged flow fields of URANS and SAS computations are small. Comparison with PIV shows good agreement for the design point and larger differences at part load. The main advantage of the turbulence resolving model is a better agreement of amplitudes in the velocity spectrum and the resolution of unstable flow patterns. The computational costs of SAS are ,however, much higher, since a fine grid is required to use the potential of the model to resolve instabilities of the flow field.

INTRODUCTION

The understanding and prediction of unsteady flow features is of increasing importance for the development and design process of turbomachines. The main problems of unsteadiness in the machine are reduced performance, noise and flow-induced vibrations. The focus of this paper is to compare different approaches of turbulence modelling with respect to experimental results. Since it

is well known that unsteady RANS models often fail to predict flow instabilities a turbulence resolving model is applied for the computations and compared to URANS simulations.

Since unsteady effects in turbomachines are of vital importance for the design process, numerous investigations were conducted in the past. There are several unsteady phenomena occurring at different length and time scales [1], such as turbulence, rotor-stator interaction and instabilities like rotating stall or surge. Small scale turbulent fluctuations of velocity and pressure are present at any operating point and are not regarded to be the main source of flow-induced vibrations. Nevertheless, turbulence of course influences large scale motion and plays an important role for noise generation. The amplitudes of pressure fluctuations are expected to be much higher for rotor-stator interaction. Much of the research of unsteady effects in turbomachinery is focused on rotor-stator interaction.

Beside excitation due to the rotor-stator effect, which appears at a known excitation frequency, flow instabilities may lead to dynamic forces with unknown excitation frequencies. The rotating stall phenomenon is a prominent example, which leads to severe dynamic loads especially for axial and centrifugal compressors. It is often characterised by a sudden drop in machine performance. An overview of existing studies is given by Pampreen [2]. The stall is induced by misalignment of the flow at part load. This leads to seperation on the suction side of the blade leading edge. A further reduction of the flow rate leads to an extension of the stalled region. Due to a blockage of the flow channel by the stall the flow is directed to the adjacent channels, where the flow is stabilised. At a certain critical flow rate the stall will begin to travel against the rotational speed in relative frame of reference. Stall speeds measured in absolute frame vary from 30 to 90 % of the rotational speed [2], several stall cells may exist at the same time. There is also evidence for the existence of rotating stall in centrifugal fans [3]. It has been pointed out in that investigation, that the typical drop in pressure rise observed for compressors does not necessarily appear. In addition to the usually observed stall on the suction side, a stall on the pressure side (p-stall) has also been observed at overload [4]. Beside the unsteady flow features specified above, separation on the blades may appear depending on the operating point. Separations are often accompanied with fluctuations of the velocity and pressure field. Flow separation from the shroud is also expected due to the turning of the flow from axial to radial direction. CFD simulations also indicate a von Karman vortex shedding of the leakage flow between inlet nozzle and shroud.

Experimental investigation of unsteady turbomachinery flow is often done using hot wire anemometry or time resolved measuring of pressure fluctuations. These techniques provide a high temporal resolution, but are restricted to point measurements. The Particle Image Velocimetry enables the simultaneous measurement of a planar velocity field. Modern High-Speed PIV systems allow field measurements with frequencies in the kHz range. This technique has been succesfully applied to the measurement of rotating stall in the impeller of a centrifugal pump [5]. In a very recent investigation HS PIV has been applied to investigate rotating stall in the vaneless diffuser of a centrifugal pump [6].

EXPERIMENTAL SETUP

The fan under investigation is a centrifugal fan with 9 blades. During the measurements rotational speeds from 1000 to 2500 rpm were investigated. The dimensions of the rotor are diameters of 188 mm at leading edge and 400 mm at trailing edge. The maximum machine Reynolds number as defined in equation (1) is $1.4\ 10^6$, the reference Mach number defined with circumferential velocity at outlet Ma_{u2} is 0.14.

$$\mathrm{Re} = \frac{u_2\, D_2}{\nu} \tag{1}$$

The blade angles are 41° at leading edge and 45° at trailing edge, the blades are shaped as circular arcs. Figure 1 displays the experimental setup for the PIV measurements. The measurement area is indicated in the figure with a red rectangle. The laser sheet illuminates the measurement area from the top. Parts of the casing and the complete impeller are made from acrylic glass in order to provide optical access to the flow channel. For this reason the rotational speed is limited to 2500 rpm.

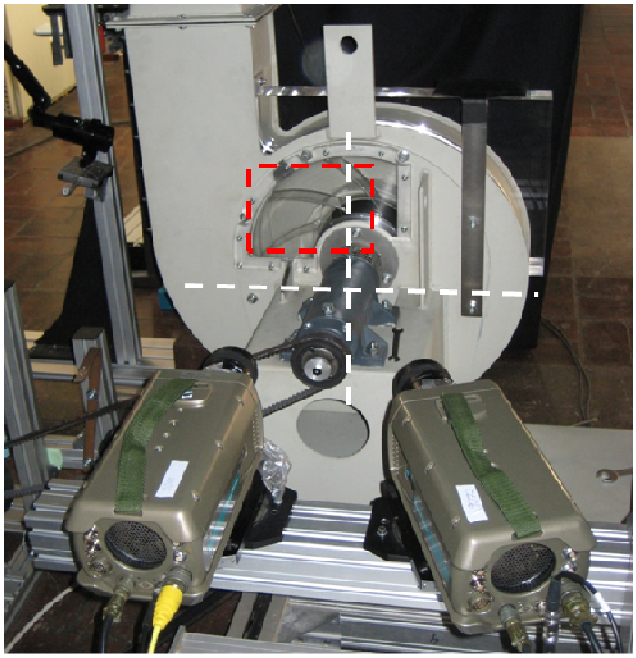

Figure 1: Experimental setup for stereoscopic PIV of inside the rotating fan impeller

As the camera takes pictures of the flow field in absolute frame of reference, the velocity in relative frame (fixed to the rotor) is calculated via subtraction of the rotational velocity in every point. A sampling frequency up to 3 kHz was achieved during the measurements. Results presented here are based on sampling with the blade passing frequency (300 Hz for 2000 rpm). The PIV measurements require a closed loop in order to avoid filtering the tracer particles. An oil dust was used as tracer.

The acquisition of the operating point is realised via measuring the pressure difference and flow rate. The mass flow rate is measured directly using a thermal mass flow measuring system. Absolute pressure and temperature are measured at the suction side to determine the fluid density. The temperature at the pressure side is also measured. The rotational speed of the fan is controlled with an electronic frequency converter. The torque at motor shaft is measured in order to obtain the efficiency of the fan. In order to minimise optical obstruction for the PIV measurements on the rear side of the impeller, the impeller shaft is driven by a synchronous belt.

NUMERICAL MODELLING

A full 3D numerical model of the fluid volume is analysed using CFD. For all computations the general purpose CFD code ANSYS CFX 12 was used. The computational model contains three parts. There is a stationary inlet domain, the rotating impeller and a stationary volute casing. Two different grids are applied to analyse the dependence on grid resolution. The block structured grid consists of 4.6 million nodes for grid 1 and 12.7 million for grid 2. The large size of the computational models requires High Performance Computing resources. Most of the computations were conducted on the North-German Supercomputing Alliance (HLRN) in Hannover with up to 96 CPUs. Despite the massive usage of parallelisation computation times are in the range of 40 hours per rotor revolution for grid 2.

Since the Mach number is low for the rotational speeds considered, the density of air was set constant according to the value measured at the inlet. The inlet is placed 5 diameters upstream the rotor, the 1/7 power law for the axial velocity was applied as boundary condition which is very easy to scale to a given flow rate. The following turbulent boundary conditions were specified at the inlet: turbulent length scale 1/20 of inlet diameter and 5 % turbulence intensity. Velocity profiles in vertical and horizontal direction were measured using LDA in order to check the inlet boundary conditions. Only little deviations from a rotational symmetric profile were found, depending on the operating point. The steady state computations did not converge better than 5×10^{-5} for the rms (root mean square) value of the residuals. For the transient computations residuals were reduced below 1×10^{-5}. Comparison of steady state results showed differences less than 2 % for pressure rise and less than 1 % for efficiency. The influence is even less for transient simulations. A comparison is listed in Table 1. A qualitative difference for the models was observed for the flow in the wake of the clearance between rotor and inlet nozzle. Only the SAS model on the fine grid is able to resolve an unsteady vortex shedding in that region. The SST computation produces a stable solution on both grids.

Table 1: Influence of grid size on performance parameters at design point; steady state and transient simulation using SST model

	nodes	**Δp [Pa]**	**η [%]**
grid 1	$4.6\ 10^6$	831	75.3
grid 2	$12.7\ 10^6$	817	74.6
grid 1, transient	$4.6\ 10^6$	882	76.8
grid 2, transient	$12.7\ 10^6$	875	76.4

For transient simulations an implicit second order integration scheme was used, which allows large Courant numbers without affecting numerical stability. For turbulence resolving models Courant numbers smaller than one should be achieved in the area of interest [7]. The time step was chosen such that one blade pitch is resolved with 2^n time steps. This is advantageous for the FFT analysis shown later. In addition the number of time steps saved to the disk can be doubled or halved keeping the sampling at blade passing frequency. One full rotor revolution is resolved with 576 steps for grid 1 and 1152 steps for grid 2 respectively. With such a relatively fine temporal resolution Courant numbers smaller than one are achieved for the largest portion of the channel excluding small regions near leading and trailing edge. Due to the enormous requirements of disk space only 72 steps per revolution were saved to disk.

Turbulence modelling

The potential of different turbulence models is a major issue of the present study. Three different approaches have been applied, steady state RANS (if applicable, depending on the operating point) URANS and SAS. The base turbulence model for all different approaches is the widely applied SST model. The SAS approach very much behaves like the more common DES (Detached Eddy Simulation), which is a hybrid LES / RANS model. The advantage of such kind of model is, that in case of sufficient temporal and spatial resolution, at least a part of the turbulent motion is resolved in regions of interest like wakes or separation bubbles. Compared to a full LES (Large Eddy Simulation) the grid resolution is very much reduced, since attached boundary layers are treated in RANS mode. This requires a fine grid only in the direction normal to the wall. A number of hybrid models have been developed in the past; a broad review is given in the work of Fröhlich and von Terzi [8]. Such advanced turbulence models are increasingly applied since the availability of High Performance Computing resources increases. Applications of hybrid LES RANS models to

turbomachine simulations are found in the literature [9, 10]. The SAS model has been successfully applied to a centrifugal pump [11]. It has been pointed out in that paper, that sufficient grid resolution in the LES region is required to obtain rotating stall frequency in agreement with measurments. Complex geometries are an ideal candidate for turbulence resolving models since LES is not feasible in most of such cases due to the still enormous computational time required.

A well known disadvantage of the first DES model of Spalart [12] is the strong dependence on the grid resolution. If the grid is refined in the wall parallel direction, so called Modelled Stress Depletion (MSD) may occur which may lead to grid induced separation. Variants like Delayed DES have been developed which minimise this problem, but do not resolve it completely [13]. Indeed SAS is an advanced URANS model, since the grid size is not involved for filtering. This is essential for Large Eddy Simulations or hybrid turbulence models, for that reason SAS should not be called "hybrid RANS LES". The advantage of SAS compared to DES is, that there is no switch between LES and RANS model. In DES this switching can be controlled by choosing an appropriate grid size, which also leads to strong dependency on the grid. The introduction of the von Karman length as a length scale into the turbulence transport equation in the SAS approach enables the model to distinguish between stable and unstable regions of the flow. In unstable regions the eddy viscosity and with it the damping of turbulent motion is reduced. Details of the model are found in the literature and will not be presented here [14]. Since there is not so much experience with the SAS model a validation with experimental results is necessary to evaluate its potential.

EXPERIMENTAL AND NUMERICAL RESULTS

Machine performance

In this section results of experiments and simulations are presented. First of all a comparison of performance curves is shown for the rotational speed of 2000 rpm. The figure also indicates the combined measurement uncertainty of pressure rise and flow rate. In order to account for the variation of inlet density during the measurements, the pressure rise is calculated for a reference density of 1.189 kg/m³. All computational results were obtained on the fine grid.

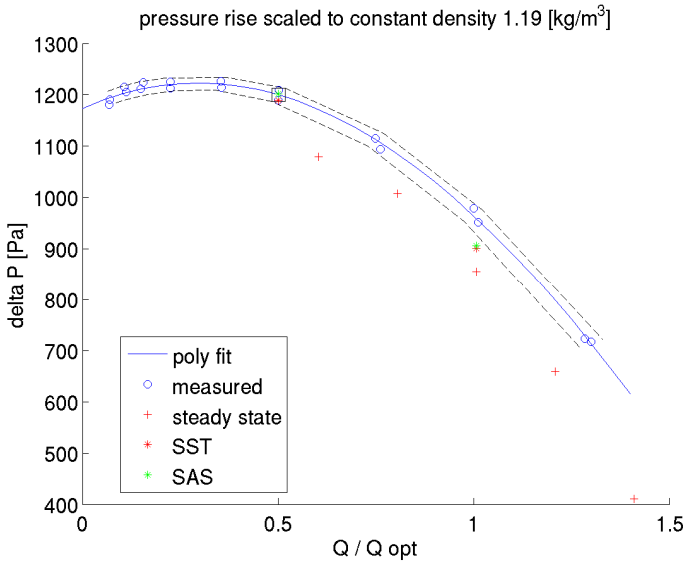

Figure 2: Performance curve including measurement uncertainty

As shown in Figure 2 the machine exhibits a stable operation down to very low flow rates less than 10 % of the nominal value without any drop in performance. The computed pressure rise for steady

state simulations is below the measured value. A transient simulation gives much better agreement with measurements. The difference between SAS and SST model for integral performance is low. The result of both models agrees with the measurements at 50 % part load within the range of uncertainty. At design point pressure rise is slightly below the uncertainty band. Due to the scatter of torque measurements induced by the belt, efficiency cannot be measured accurately.

Velocity fields

The PIV measurements provide the three components of the velocity time resolved in a measurement plane located at middle height of the flow channel. The velocity field inside one full blade channel near the blade tongue is visualised as indicated in Figure 1. All results presented are based on time averaged velocity fields. Measurement results of the velocity component normal to the measurement plane show sometimes unphysically high values. For that reason only the in plane components of velocity will be presented here. This error is attributed to refraction at the transparent window. Reflection and diffraction also contribute to the error, which is amplified in the third direction. In addition droplets of the tracer (DEHS - Di-Ethyl-Hexyl-Sebacat) settle on the window and the impeller. Although the fan was regularly cleaned, the pollution of the optical access additionally increases the measurement uncertainty. It also known from the literature, that the errors amplify for velocity component measured normal to the measurement plane [15, 16]. Figure 3 shows the development of the time averaged flow field from design flow rate down to 7 % of the nominal value. The contour plot indicates the magnitude of velocity. Already at the design point measurements indicate a thickening of the boundary layer on the suction side near the blade trailing edge. This is displayed more clearly in the CFD results, which show separation of the flow near to the blade surface in that region. The corresponding separation bubble is located at the boundary of the measured region and could not be resolved in the measurements. Reduction of the flow rate to 75 % leads to an increased region of low velocity on the suction side. The flow shows a jet like behaviour in the middle of the flow channel. At 50 % part load the size of the separation on the suction side has very much increased and is clearly visible in the vector plot. The suction side of the channel is blocked and drives the flow to the pressure side of the channel. At 23 % part load the size of the vortex has increased and blocks most of the channel. In addition a second counter rotating vortex begins to develop on the pressure side. The flow field measured is not representative for other channels due to the vicinity of the volute tongue. A further reduction of the flow rate leads to an increased size of the second vortex, which dominates the flow at very low flow rate of 7 % part load. Since there is nearly no mass flow through the channel the appearance of a vortex rotating against the rotor direction is in agreement with the relative channel vortex in the theory of turbomachinery.

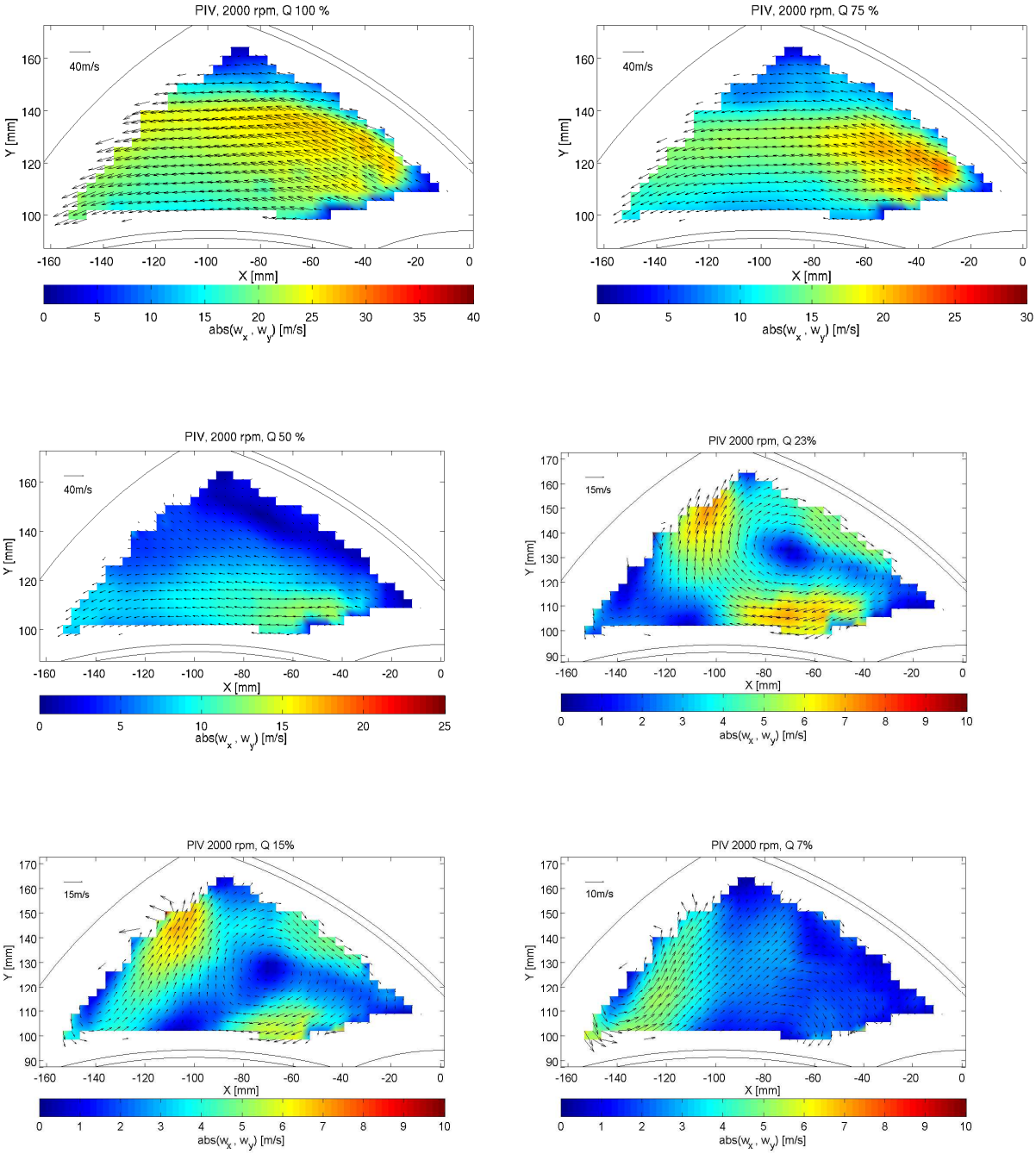

Figure 3: Development of the measured velocity field from design point to very low part load

The validation of CFD computations is done using the measured velocity fields. The comparison also includes the topology of the flow field which, is characterised by the position of vortex centres in the mean velocity field. Due to the large computational time only two operating points are available for comparison with transient CFD, which are the design point and 50 % part load. For the comparison the CFD data are mapped onto coordinates of the measurement points and averaged in time. The time averaged flow fields for the design point are displayed in Figure 4. In this operating point the swirl center of the separation zone is located very close to the blade surface near the trailing edge. SAS as well as SST computation show a good agreement of the velocity field. The magnitude of velocity near to the suction side is, however, over predicted.

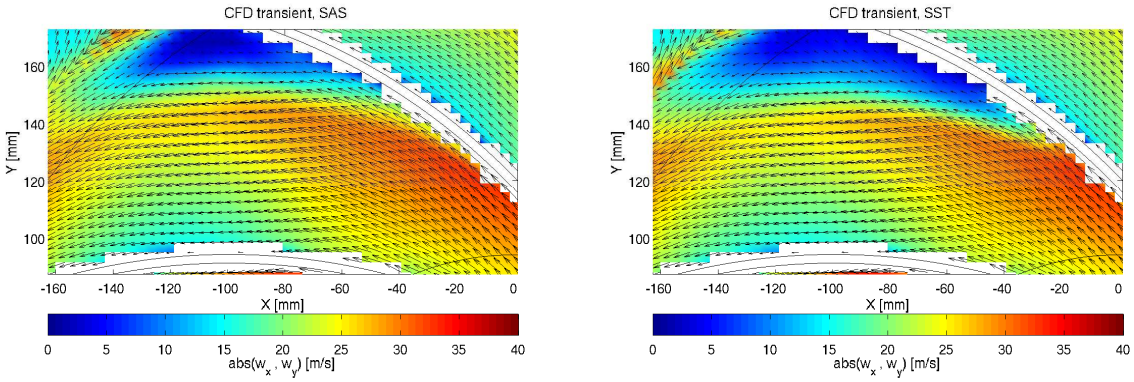

Figure 4: Comparison of computed velocity fields in the centre plane of the rotor at design point (SAS left, SST right), PIV results are shown in Figure 3

The region of low velocity near the trailing edge is larger for the SST computation. All results shown are obtained from averaging 5 rotor revolutions on the fine grid. The agreement is worse for part load operation (Figure 5). The CFD computations show a jet like flow in the middle of the channel and a separation on the suction side near to the leading edge. Magnitude of the velocity in that region is over predicted for both models. The location of the separation zone is further downstream in the PIV measurements. Simulation results indicate only little difference of the time averaged flow field for SAS and SST computation. Nevertheless the instantaneous flow fields differ a lot. As expected the SAS model resolves large scale turbulent motion, which leads to strongly unsteady velocity field. The SST model shows only small temporal deviations from the averaged flow field shown in Figure 5.

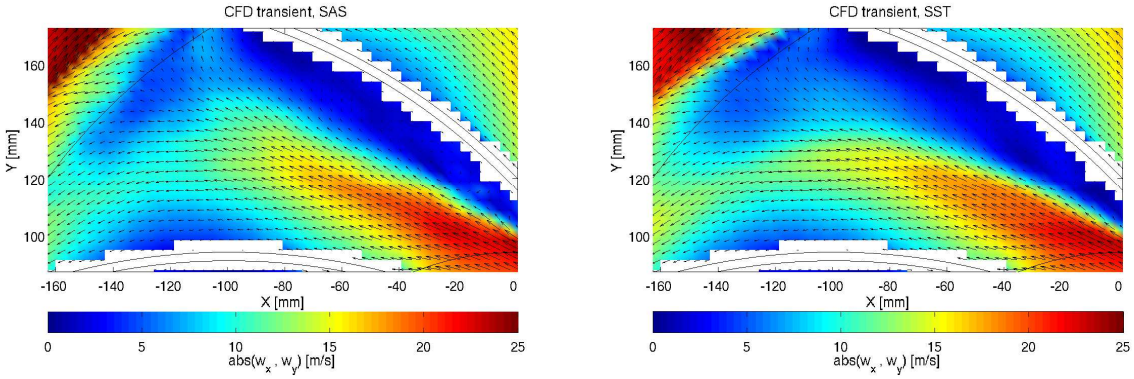

Figure 5: Comparison of velocity fields in the centre plane of the rotor for 50% load (SAS left, SST right), PIV results are shown in Figure 3

Spectra of the velocity and integral forces on the rotor

In order to obtain possible excitation frequencies induced by fluctuations of the flow field a Fourier transformation of velocity was done. As input signal a complex velocity derived in cylindrical coordinates is used according to equation (2). With this definition the magnitudes of the velocity as well as the flow angle is used, which increases the signal to noise ratio. The spectra of every point in the measurement plane with a complete time history were averaged; the result is displayed in Figure 7 in comparison with the CFD data.

$$W(t) = w_{rad}(t) + j\, w_u(t) \tag{2}$$

The measured spectrum indicates the rotational speed in all operating points. In addition a value of roughly 60-70 % of the rotational frequency is observed for flow rates smaller than ca. 50 % part load. This is the case for nearly all rotational speeds analysed apart from 2500 rpm. At 2500 rpm the spectra did not show a peak in the range of 70 % rotational speed at any operating point. The number of images was limited to 128 due to the large image processing time and disk space required by the stereoscopic PIV. This results in a rather coarse resolution of 7 % of the rotational frequency.

The operating point chosen was 50 % of nominal flow rate. At the design point the measured spectra show only the rotational speed, for that reason a spectrum was not evaluated from CFD. The physical time in the computations was 7 revolutions for the spectra presented. An initial time span of 5 revolutions was skipped for evaluation. The data shown corresponds to the fine grid computation. The maximum amplitude of the measurements spectrum is located at 33 Hz, which corresponds to the rotational speed. Another peak is visible at 23 Hz; this maximum is also found in the SST computation. The corresponding peak for the SAS model is at a slightly higher frequency. Note that due to the small physical time the resolution in frequency is only 4.7 Hz for the computations. An improvement is possible, but requires long computation time. The level of amplitudes is too low for the SST model but higher for the SAS model. Especially the fluctuations due to instable flow are not computed accurately with the RANS model. For that reason the transient forces are expected to be better predicted with the SAS model. However the differences in integral forces are small, the predicted time averaged torque differs only by less than 2 % for both models.

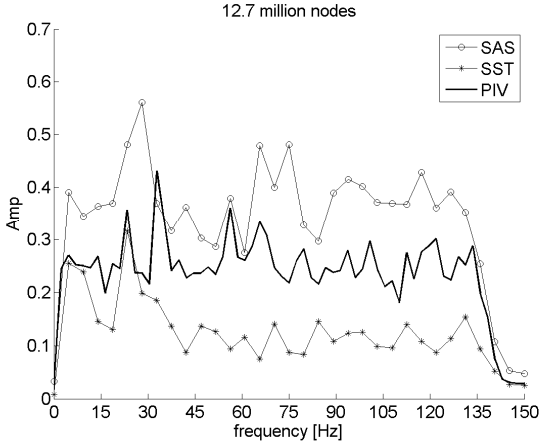

Figure 6: Averaged spectrum of complex velocity; CFD vs. PIV

The spectra of the integrated forces on the rotor surface are shown in Figure 7. The forces include pressure and viscous forces. As for the velocity a complex input signal for the force is defined as:

$$F(t) = F_x(t) + j\, F_y(t) \tag{3}$$

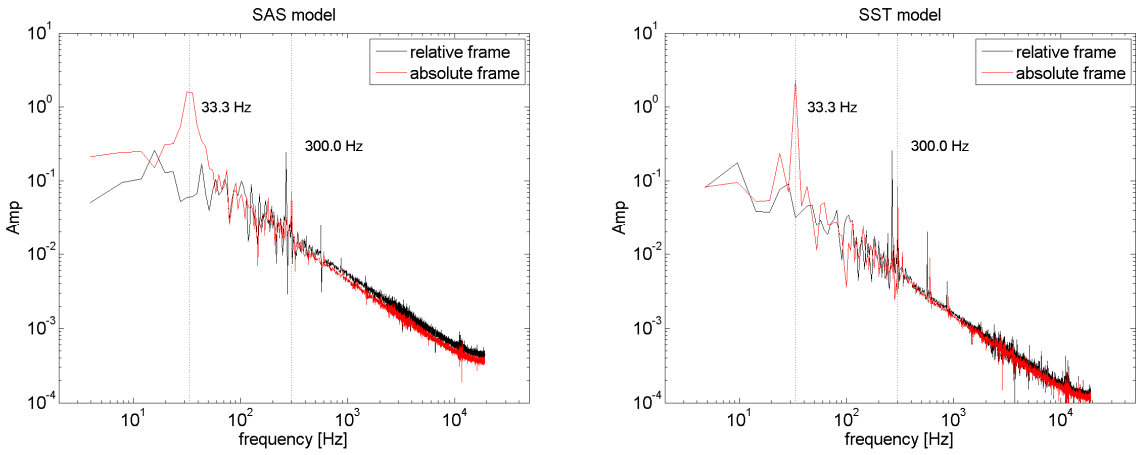

Figure 7: Spectrum of integrated force on the impeller

It is possible to evaluate the forces in relative or in absolute frame of reference. Important for the excitation of impeller vibration is the evaluation in relative frame. As expected the major excitation frequency is the rotational speed due to the interaction with the spiral tongue. In absolute frame the blade passing frequency (z x f_{rot}; 300 Hz) results in another important peak. This frequency has to be considered for structural vibrations of stationary components of the machine. In rotating frame of reference the corresponding excitation frequency is the blade passing frequency minus the rotational speed ((z-1) x f_{rot}; 267 Hz). This is simply the result of transformation from absolute to relative frame of reference.

There is some difference for both models. The SST model shows the dominant peaks more clearly. Since the time scale of these fluctuations is separated from turbulent scales a RANS model is expected to reproduce them properly. The turbulence resolving model has some more content due to turbulent fluctuations. In general amplitudes of forces are higher with SAS apart from the two dominant peaks. This is especially true for high frequencies. In relative frame a frequency of 16 Hz is observed with SAS which is attributed to instability of the fluid flow. It is also possible to record the local pressure signal which can be used as input for structural simulation. This work is in progress for an impeller made from steel.

CONCLUSIONS

The main conclusion of the work is that the difference of the time averaged velocity fields is rather small for SAS and SST. The SAS model requires a fine grid to resolve large scale turbulent structures. Even the grid with 12.7 million points may not sufficient. In addition the computational time for same time step and grid size is up to 40% larger for SAS compared to SST. This is mainly due to the larger number of iterations within one time step. An advantage of the turbulence resolving model is the prediction of velocity fluctuations. The amplitudes in the velocity spectrum correspond better to the measured values. Instabilities of the flow like vortex shedding in the wake of rotor-stator clearance are not resolved with the SST model. For that reason the model is regarded to be the better choice for fluid-structure interaction.

ACKNOWLEDGEMENT

This work was funded by the AiF (Arbeitsgemeinschaft industrieller Forschungsvereinigungen) Germany, grant number 16406BG/1. The computations were performed on the supercomputer HLRN-II of the North-German Supercomputing Alliance (HLRN, www.hlrn.de). The fan was made

available for the measurements by Piller Industrial Fans GmbH, Germany. The authors would like to thank all institutions for their kind support of this investigation.

BIBLIOGRAPHY

[1] Greitzer, E. M. *An introduction to unsteady flow in turbomachines*. in "Thermodynamics and Fluid Mechanics of Turbomachinery", Vol. 2. Dordrecht : Martinus Nijhoff Publishers, pp. 967-1024, **1985**

[2] Pampreen, R.C. *Compressor surge and stall.* Norwich Vt : Concepts ETI, **1993**.

[3] Chen, P., et al. *Unstable flow in centrifugal fans.* Journal of Fluids Engineering. pp. 128-133, **1996**

[4] Madhavan, S. and Wright, H. *Rotating stall caused by pressure surface separation on centrifugal fan blades.* Journal of Engineering for Gas Turbines and Power. pp. 775-781, **1985**

[5] Krause, N., Zähringer, K. and Pap, E. *Time-resolved particle image velocimetry for the investigation of rotating stall in a radial pump.* Experiments in Fluids. pp. 192-201, **2005**

[6] Dazin, A., et al. - *High-speed stereoscopic PIV study of rotating instabilities in a radial vaneless diffuser.* Experiments in Fluids. pp. 83-93, **2011**.

[7] Spalart, P. - *Young-persons guide to Detached-Eddy Simulation grids*. NASA Report CR-2001-211032, **2001**

[8] Fröhlich, J. and von Terzi, D. Hybrid *LES/RANS methods for the simulation of turbulent flows.* Progress in Aerospace Sciences. pp. 349-377, **2008**

[9] Feng, J., Benra, F.-K. and Dohmen, H.J. *Unsteady flow visualization at part-load conditions of a radial diffuser pump: by PIV and CFD*. Journal of Visualization. pp. 65-72, **2009**

[10] Iwakiri, K., et al. *Unsteady and three-dimensional flow phenomena in a transsonic centrifugal compressor at rotating stall*. Proceedings of the ASME Turbo Expo, Orlando. pp. 1611-1622, **2009**

[11] Lucius, A. and Brenner, G. *Numerical simulation and evaluation of velocity fluctuations during rotating stall of a centrifugal pump*. Journal of Fluids Engineering. pp. 081102-8, **2011**

[12] Spalart, P. *Comments on the Feasibility of LES for Wings and on a hybrid RANS LES approach*. Advances in DNS/LES: Proceedings of the 1st. AFSOR International Conference on DNS/LES, Rushton, **1997**

[13] Spalart, P.R., et al. *A new version of detached-eddy simulation resistant to ambiguous grid densities. Theoretical Computational Fluid Dynamics*. pp. 181-195, **2006**

[14] Menter, F.R. and Egorov, Y. *A scale-adaptive simulation model using two equation models.* AIAA Paper 2005-1095, **2005**

[15] Thorwarth, J. *Dreidimensionales Hochgeschwindigkeits-PIV mit einem Ein-Kamera-System.* 4. JuWi Treffen TU München, **2002**

[16] Willert, C. *Stereoscopic digital particle image velocimetry for application in wind tunnel flows*. Measurement Science and Technology. pp. 1465-1479, **1997**